Attractor comparison analysis for characterizing vertical upward oil–gas–water three-phase flow*

Zhao Jun-Ying(赵俊英)[a)b)], Jin Ning-De(金宁德)[a)†], Gao Zhong-Ke(高忠科)[a)], Du Meng(杜 萌)[a)], and Wang Zhen-Ya(王振亚)[a)]

[a)] *School of Electrical Engineering and Automation, Tianjin University, Tianjin* 300072, *China*
[b)] *Electronic Engineering Department, Tianjin Vocational College of Electronics & Information, Tianjin* 300350, *China*

(Received 12 May 2013; revised manuscript received 16 June 2013; published online 24 January 2014)

We investigate the dynamic characteristics of oil–gas–water three-phase flow in terms of chaotic attractor comparison. In particular, we extract a statistic to characterize the dynamical difference in attractor probability distribution. We first take time series from Logistic chaotic system with different parameters as examples to demonstrate the effectiveness of the method. Then we use this method to investigate the experimental signals from oil–gas–water three-phase flow. The results indicate that the extracted statistic is very sensitive to the change of flow parameters and can gain a quantitatively insight into the dynamic characteristics of different flow patterns.

Keywords: oil–gas–water three-phase flow, fluid dynamics, attractor comparison

PACS: 47.55.Ca, 47.52.+j **DOI:** 10.1088/1674-1056/23/3/034702

1. Introduction

Oil–gas–water three-phase flow widely exists in oil well production, petroleum storage and transportation systems. Owing to the interaction between the three phases of oil, gas, and water, such as fluid turbulence, local relative movements, the oil–gas–water three-phase flows are very complex and varied with individual phase flow parameters, which are usually called difficult fluid flows. Therefore, traditional theoretical analyses based on mathematical analytical calculations or fluid models have many limitations in uncovering the nonlinear dynamics of multi-phase flow,[1,2] and it is rather difficult to directly obtain the dynamic characteristics by numerical simulation.[3,4] The current methods applied to multi-phase flow such as power spectrum analysis,[5,6] time-frequency representation,[7,8] artificial intelligence,[9,10] nonlinear analysis,[11–16] and attractor morphology[17–19] have made great progress in uncovering the fluid dynamics from their own respect. However, the power spectrum analysis and the time-frequency domain representation always lose phase information of the system, and those methods usually need a long time series to obtain a reliable result; artificial intelligence can effectively identify flow patterns, but it is rather difficult to uncover the mechanism governing the transition of multi-phase flow; although the traditional nonlinear analysis methods can provide one or more dynamical characteristics of the system, these methods always neglect the dynamical relations between attractor interior vectors.

The attractor comparison method[20] has been applied to the early warning agglomeration of fluidized beds and the detection of foam formation in bubble columns by researchers from different fields.[21–25] The attractor comparison method takes each vector's local probability distribution into account and can observe the changes of the attractor as a whole. More importantly, it can quantitatively characterize the differences between attractors. In this regard, according to the conductance signals measured from oil–gas–water three-phase flow experiment, we employ the attractor comparison method to investigate oil–gas–water three-phase flow. The results yield a quantitative insight into the dynamic characteristics of difficult fluid flows.

2. Attractor comparison analysis of chaotic time series

2.1. Method

The main idea of the attractor comparison method[20] is to construct a general square distance Q between multidimensional distributions, the square distance reflects the absolute difference between attractors. From this point of view, the distance Q between two identical delay vectors is zero. To obtain a general quantity, we use the statistic S to present a quantitative description of the differences.

Assume $x_k(k = 1,2,3,\ldots,N_x)$ as the reference time series and $y_k(k = 1,2,3,\ldots,N_y)$ as the evaluation time series, we obtain $\boldsymbol{X}_i = (x_i, x_{i+\tau}, \ldots, x_{i+(m-1)\tau})$ and $\boldsymbol{Y}_i = (y_i, y_{i+\tau}, \ldots, y_{i+(m-1)\tau})$ after phase space reconstruction with embedding dimension m and delay time τ, and the total numbers of the reconstructed vectors are M_x and M_y respectively, and the probability distributions are $\rho_x(\boldsymbol{X}_i)$ and $\rho_y(\boldsymbol{Y}_i)$.

*Project supported by the National Natural Science Foundation of China (Grant Nos. 41174109 and 61104148), the National Science and Technology Major Project of the Ministry of Science and Technology of China (Grant No. 2011ZX05020-006), and the Tianjin City High School Science and Technology Fund Planning Project, China (Grant No. 20130718).

†Corresponding author. E-mail: ndjin@tju.edu.cn

© 2014 Chinese Physical Society and IOP Publishing Ltd

Define the smoothed probability distribution $\rho'_x(\boldsymbol{X}_i)$ as the convolution of $\rho_x(\boldsymbol{X}_i)$ and the Gaussian kernel

$$\rho'_x(\boldsymbol{X}_i) = \int \rho_x(\boldsymbol{R})(d\sqrt{2\pi})^{-m} \mathrm{e}^{-|\boldsymbol{X}_i-\boldsymbol{R}|/(2d^2)} \mathrm{d}\boldsymbol{R}, \quad (1)$$

where the band width d is a fixed length scale, the smoothed distribution $\rho'_y(\boldsymbol{Y}_i)$ can be calculated in a similar way. The transformation means that the points in the state space are not represented with probability one at the positions of their exact values and probability zero elsewhere, but that they have a certain Gaussian probability distribution around their actual values.

According to the definition of the smoothed probability distribution, we obtain the squared distance Q of the two smoothed distributions as

$$Q = (2d\sqrt{\pi})^m \int \left[\rho'_x(\boldsymbol{R}) - \rho'_y(\boldsymbol{R})\right]^2 \mathrm{d}\boldsymbol{R}. \quad (2)$$

To calculate an estimator $\hat{Q}$ for Q, the two sets $\boldsymbol{X}_i$ and $\boldsymbol{Y}_i$ are combined as a new set $\boldsymbol{Z}_i$ which is expressed as

$$\boldsymbol{Z}_i = \begin{cases} \boldsymbol{X}_i, & (1 \le i \le M_x), \\ \boldsymbol{Y}_{i-M_x}, & (M_x < i \le M_s), \end{cases} \quad (3)$$

where $M_s = M_x + M_y$.

To eliminate the dependence between subsequent delay vectors, Diks *et al.*[20] divided the (i, j)-plane representing all possible pairs of $\boldsymbol{Z}_i$ and $\boldsymbol{Z}_j$ in $N \times N$ squares of size $L \times L$, by segment length L that is so large that pairs with $|i-j| \ge L$ are not correlated with each other. For each square, an average value

$$H_{pq} = \frac{1}{L^2} \sum_{i=1}^{L} \sum_{j=1}^{L} h(\boldsymbol{Z}_{(p-1)L+i}, \boldsymbol{Z}_{(q-1)L+j}) \quad (4)$$

is calculated, and

$$h(\boldsymbol{Z}_i, \boldsymbol{Z}_j) = \mathrm{e}^{-|\boldsymbol{Z}_i-\boldsymbol{Z}_j|^2/(4d^2)}. \quad (5)$$

Suppose that there are N_1 and N_2 squares in the reference set and the evaluation set respectively, p and q are the indices, then we will obtain the unbiased estimator of Q as

$$\hat{Q} = \frac{2}{N_1(N_1-1)} \sum\sum_{1 \le p < q \le N_1} H_{pq} + \frac{2}{N_2(N_2-1)} \sum\sum_{N_1+1 \le p < q \le N} H_{pq} - \frac{2}{N_1 N_2} \sum_{p=1}^{N_1} \sum_{q=N_1+1}^{N} H_{pq}. \quad (6)$$

The larger the difference between the two sets of delay vectors, the larger the square distance $\hat{Q}$ between them will be. To know whether a certain value of $\hat{Q}$ indicates a significant difference between two delay vectors, an estimate of the variance V_c is given as

$$V_c(\hat{Q}) = \frac{4(N-1)(N-2)}{N_1(N_1-1)N_2(N_2-1)N(N-3)} \sum\sum_{1 \le p < q \le N} \psi_{pq}^2, \quad (7)$$

in which

$$\psi_{pq} = \hbar_{pq} - g_p - g_q, \quad (8)$$

$$\hbar_{pq} = H_{pq} - \frac{2}{N(N-1)} \sum\sum_{1 \le p' < q' \le N} H_{p'q'}, \quad (9)$$

$$g_p = \frac{1}{N-2} \sum_{\substack{q \\ p \ne q}} \hbar_{pq}. \quad (10)$$

The statistic S is defined as

$$S = \frac{\hat{Q}}{\sqrt{V_c(\hat{Q})}}. \quad (11)$$

In fact, Pukkelsheim *et al.*[26] have provided a three-sigma rule which shows that for any unimodal probability density, the probability for values larger than three times the standard deviation is smaller than 5%. According to the three-sigma rule,[26] we obtain the conclusion that the S value larger than 3 indicates a significant difference between the two series with more than 95% confidence. In addition, Diks *et al.*[20] conducted numerical simulations and indicated that the confidence level is about 98 to 99%, van Ommen *et al.*[21] applied the method to the fluidized beds and confirmed this conclusion.

A comparison of the statistic S with the traditional probability density method or the power spectral density method shows that the statistic S considers more of the entire structure of the attractor and the relevance of the time series, and the S value can better reflect the differences between attractors.

2.2. Probability distribution differences of a typical chaotic time series

We obtain a time series from the Logistic function as follows:

$$x_{n+1} = \lambda x_n (1 - x_n), \quad (12)$$

as shown in Fig. 1(a), where $\lambda = 3.905$, and $n \in [201, 400]$ is a sub-time series serving as a reference data set as shown in Fig. 1(b).

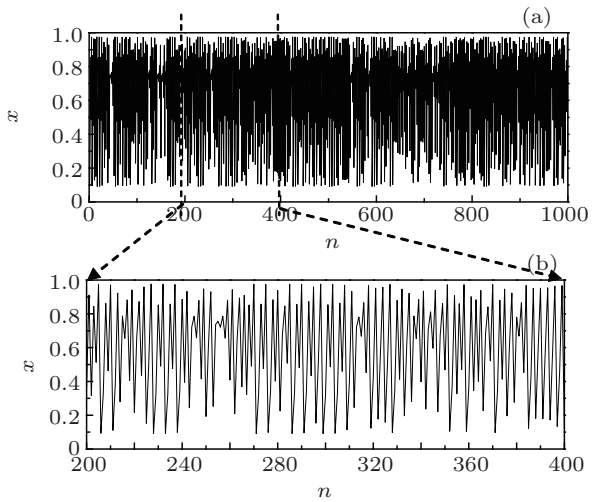


Fig. 1. Time series from Logistic system with (a) a time series for $n \in [1, 1000]$, and (b) a sub-time series for $n \in [201, 400]$ serving as reference data set.

We obtain some logistic time series of length 1000 as the evaluation time series with the parameter λ changing in steps of 0.01. We then divide each time series into 5 parts each with a length of 200. Figure 2 shows the first 200 points of each λ value. Finally we employ the average S values (denoted as $S[-]$) as the comparison results among these different time series. Figure 3 shows the distribution of $S[-]$ value with respect to parameter λ, where the embedding dimension $m = 3$, time window $\tau = 1$, band width $d = 0.01$, and segment length $L = 20$. As can be seen from the figure, the $S[-]$ value is larger than 3, when $\lambda \geq 3.925$, indicating that there appears a significant change in the dynamical mechanism.

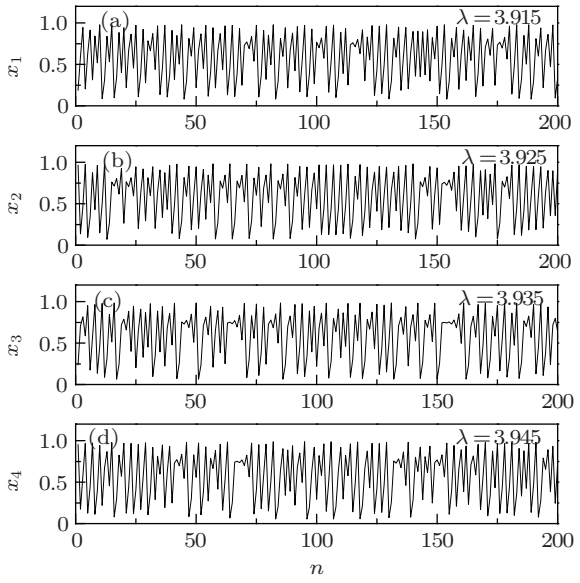


Fig. 2. Different logistic time series to be evaluated. (a) $\lambda = 3.915$, (b) $\lambda = 3.925$, (c) $\lambda = 3.935$, (d) $\lambda = 3.945$.

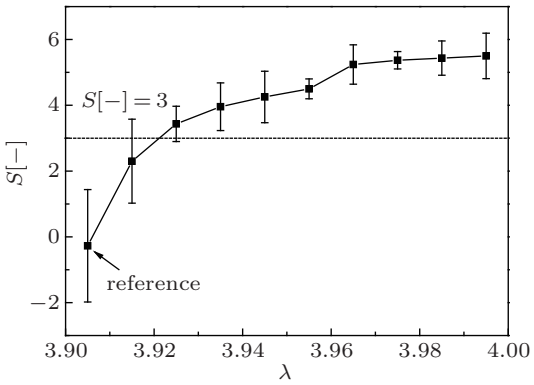


Fig. 3. Distribution of $S[-]$ value with respect to parameter λ.

3. Data acquisition from oil–gas–water three-phase flow experiment

An oil–gas–water three-phase flow experiment in a 125-mm diameter vertical upward transparent Plexiglas pipe is carried out in the multiphase flow loop of Tianjin University, and the conductance fluctuating signals of different flow patterns are acquired from the VMEA sensors.[27] The ranges of the experimental flow rates are as follows: the total liquid flow rates are 20, 40, 60, and 80 m^3 per day, and the values of oil volume fraction (f_o) are mainly 0.1, 0.2, 0.3, 0.4, 0.5, 0.7, and 0.9 and the gas flow rates range from 8 to 180 m^3 per day. In the experiment, the liquid mixture flow rate (oil and water) and the ratio of oil flow rate to liquid mixture flow rate (f_o) are fixed and gas flow rate is gradually increased. Finally, we observe and define the six typical oil–gas–water flow patterns in the experiment, i.e., oil in

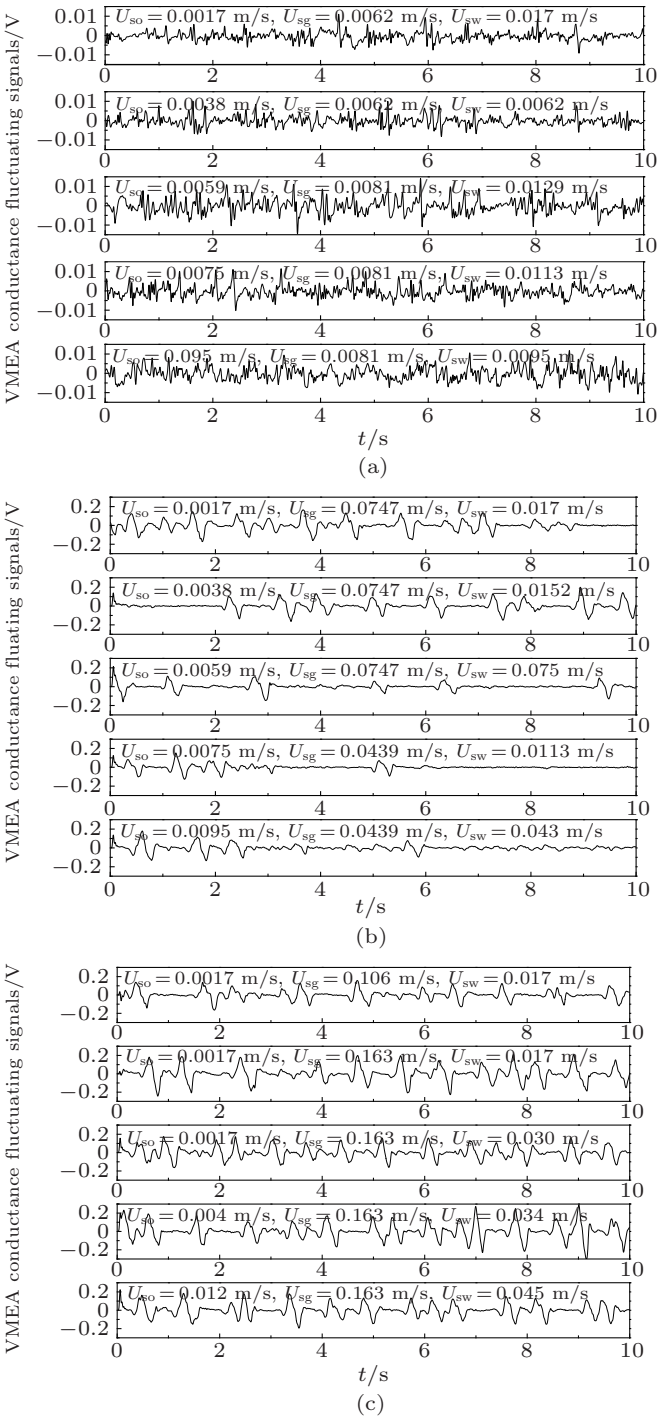


Fig. 4. Conductance fluctuating signals measured from (a) oil in water-type bubble flow, (b) oil in water-type bubble-slug transitional flow, and (c) oil in water-type slug flow.

water-type bubble flow, oil in water-type bubble-slug transitional flow, oil in water-type slug flow, emulsion-type bubble-slug transitional flow, emulsion-type slug flow, and water in oil-type slug flow. Figure 4 shows the conductance fluctuating signals for three water-dominated flow patterns. The sampling frequency is 400 Hz and the sampling data recording time for one measuring point is 50 s in the experiment.

4. Attractor comparison analysis of flow patterns

Figure 5 shows the three-dimensional (3D) attractor morphologies for three typical water-dominated flow patterns. We can see that each attractor exhibits a distinct probability distribution.

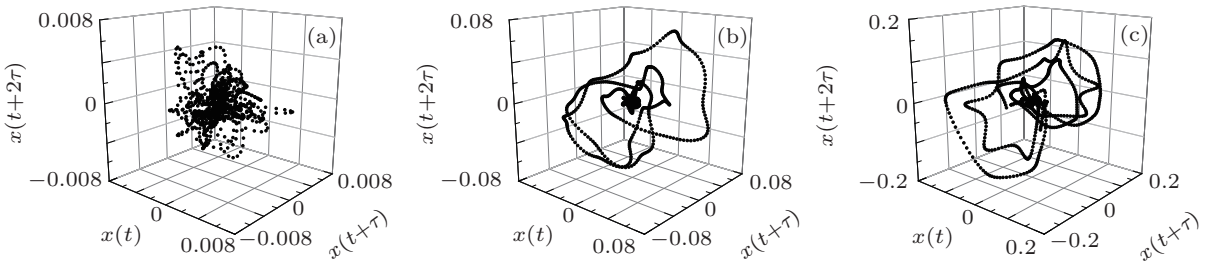


Fig. 5. Attractor morphologies for three typical flow patterns with (a) $U_{so} = 0.0017$ m/s, $U_{sg} = 0.0062$ m/s, $U_{sw} = 0.017$ m/s; (b) $U_{so} = 0.0017$ m/s, $U_{sg} = 0.0747$ m/s, $U_{sw} = 0.017$ m/s; (c) $U_{so} = 0.0017$ m/s, $U_{sg} = 0.106$ m/s, $U_{sw} = 0.017$ m/s.

4.1. Selections of parameters

We choose a signal of length 10000 (25 s) for each flow condition and divide the signal into 10 sub-signals each with a length of 1000 (2.5 s). Then we choose a stable sub-signal as a reference set, and compare other sub-signals with the reference set to obtain 10 statistic values for each flow condition. Finally, we calculate the mean value and the standard deviation of S to investigate the flow dynamical characteristics. Note that two time series measured under similar hydrodynamic conditions will present an S value close to 0, whereas a maximal S value (at least > 3) indicates that the two time series are measured from different hydrodynamic conditions. We now investigate the influences of four parameters on the performance of the method, including time window τ, embedding dimension m, band width d, and segment length L. The proper parameters will be chosen from the calculations. We choose an oil in water-type bubble flow ($U_{so} = 0.00165$ m/s, $U_{sw} = 0.017$ m/s, $U_{sg} = 0.01$ m/s) data set as the reference time series, and select another two fluctuating signals as the evaluation time series, where one evaluation time series is a similar oil in water-type bubble flow ($U_{so} = 0.00165$ m/s, $U_{sw} = 0.017$ m/s, $U_{sg} = 0.013$ m/s) signal and the other one is a time series from an oil in water-type slug flow ($U_{so} = 0.00165$ m/s, $U_{sw} = 0.017$ m/s, $U_{sg} = 0.132$ m/s). The length of all the signals are 25 s and these signals are divided into 10 sub-signals for calculation of $S[-]$. The results are shown in Fig. 6.

Figure 6(a) shows the influences of the time window τ on the calculation of the $S[-]$ value for the case of embedding dimension $m = 9$, band width $d = 0.05$, and segment length $L = 200$ ms. As can be seen, for the oil in water-type slug flow, the values of $S[-]$ are high when the time window is around 30 ms–90 ms; while for the oil in water-type bubble flow, the values of $S[-]$ are very small and almost independent of time window τ. Meanwhile, according to Takens' theory,[28] attractors of the three-phase flow will expand enough when the time window is around 70 ms–100 ms, we thus finally choose $\tau = 87.5$ ms as the proper time window.

Figure 6(b) shows the influences of the embedding dimension d on the calculation of the $S[-]$ value for the case of time window $\tau = 87.5$ ms, band width $d = 0.05$ and segment length $L = 200$ ms. As can be seen, for the oil in water-type slug flow, the values of $S[-]$ are high when the dimension m takes values between 4 to 11; while for the oil in water-type bubble flow, the values of $S[-]$ are very small and almost independent of the embedding dimension. Taking the Takens' theory[28] into consideration, we choose the embedding dimension $m = 9$.

The selection of the bandwidth d greatly influences the performance of the method.[20] If it is too small, the test will pick up local differences between the two distributions, which then leads to poor statistics. If it is too large, the delay vector distributions will be smoothed to such an extent that they become practically indistinguishable. The optimal value for the band width is expected to be found at the trade-off between these two effects. We, in Fig. 6(c), show the distribution of $S[-]$ with respect to bandwidth d for the case of time window $\tau = 87.5$ ms, embedding dimension $m = 9$ and segment length $L = 200$ ms. As can be seen, the statistic $S[-]$ decreases slowly with the up-growing of d for the oil in water-type slug flow, and there is little influence on the oil in water-type bubble flow except that d takes a too small value. Finally we select $d = 0.05$ as the standard value for the calculation of $S[-]$.

The function of segment length L is to eliminate the interaction between nearby points. It is important to take it large enough to remove dynamic correlations between successive

points in the state space. Diks *et al.*[20] stated that the power of the test is nearly optimal as long as the number of segments is not smaller than 8 and the segment length is long enough to contain several cycles of the fluctuation signal. We, in Fig. 6(d), show the distribution of $S[-]$ with respect to segment length L for the case of time window $\tau = 87.5$ ms, embedding dimension $m = 9$, and band width $d = 0.05$. As can be seen, $S[-]$ decreases with L for the oil in water-type slug flow, while $S[-]$ is almost independent of the segment length L for the oil in water-type bubble flow. According to the statements by Diks *et al.*,[20] and our test , we select $L = 150$ ms as the proper segment length for the calculation of $S[-]$.

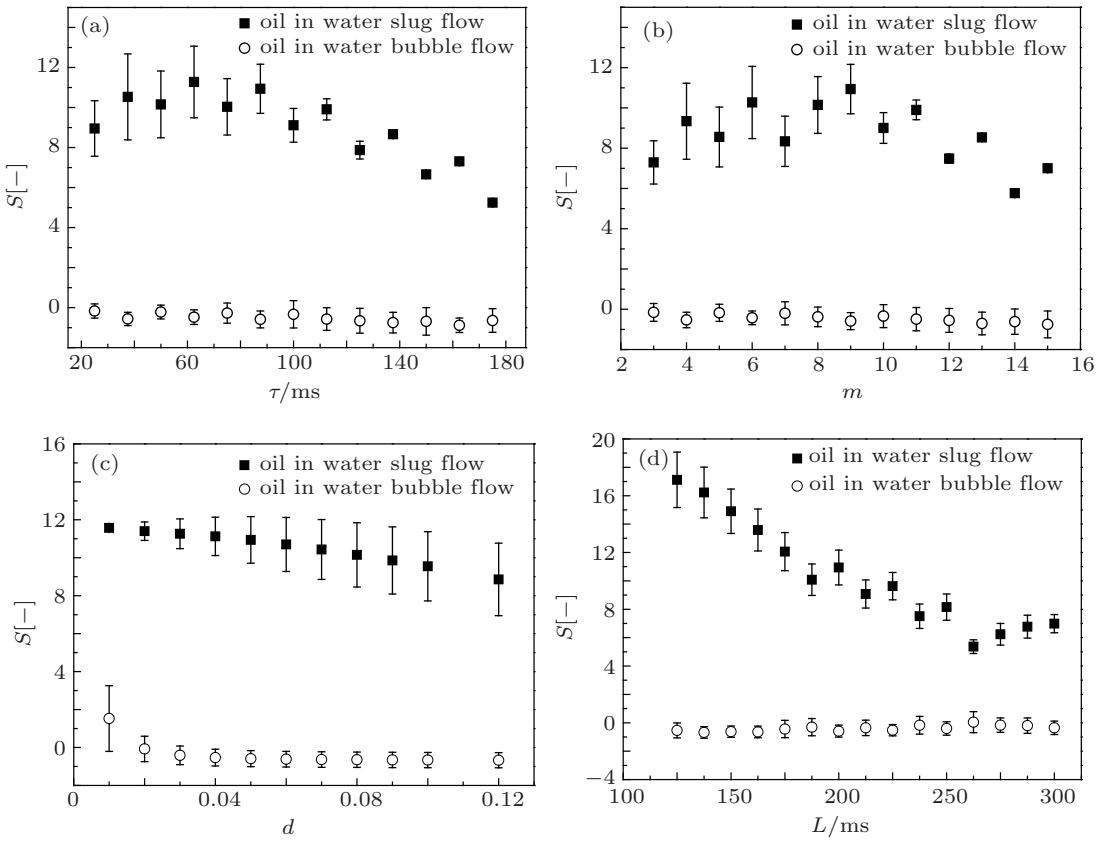


Fig. 6. Proper parameters for the calculation of $S[-]$. (a) $m = 9$, $d = 0.05$, $L = 200$ ms; (b) $\tau = 87.5$ ms, $d = 0.05$, $L = 200$ ms; (c) $\tau = 87.5$ ms, $m = 9$, $L = 200$ ms; (d) $\tau = 87.5$ ms, $m = 9$, $d = 0.05$.

In addition, when the time window τ, embedding dimension m and segment length L take relatively small values, the calculation will be too time consuming, so we choose relatively large values for these three parameters in practice. Therefore, we choose $\tau = 87.5$ ms, $m = 9$, $d = 0.05$, and $L = 150$ ms as proper parameters.

4.2. Attractor comparison analysis of three-phase flows

4.2.1. Distributions of $S[-]$ with respect to gas superficial velocity

Figure 7 shows the distributions of $S[-]$ with respect to gas superficial velocity when the liquid mixture flow rate is fixed at 20 m^3 per day, and the oil volume fraction is fixed at 10% (Fig. 7(a)) and 20% (Fig. 7(b)). As can be seen, the oil in water-type bubble flow evolves into oil in water-type slug flow with the increase of gas superficial velocity under a fixed oil volume fraction. We choose the relatively stable bubble flows as references for the calculation of $S[-]$. When the gas superficial velocity $U_{sg} \leq 0.043$ m/s, the flow pattern is the oil in water-type bubble flow, and the $S[-]$ values are less than 3, indicating that there is no significant change of the fluid mechanism; when the gas superficial velocity reaches $U_{sg} = 0.075$ m/s, due to the increase of turbulence energy, some small slugs appear and the flow pattern evolves into bubble-slug transitional flow, meanwhile, the $S[-]$ value is far larger than 3, indicating a significant change of fluid mechanism. When $U_{sg} \geq 0.1064$ m/s, the turbulence energy increases very rapidly and the flow pattern changes into a typical oil in water-type slug flow. Correspondingly, the $S[-]$ value stays near 14–16 which are greatly larger than 3, indicating that the fluid mechanism undergoes a significant change induced by the increase of turbulence energy.

The standard deviations of $S[-]$ for the oil in water-type bubble flow and oil in water-type slug flow are both small, indicating these two flow patterns are relatively stable. The

explanation of the stability of the oil in water-type bubble flow is that it occurs at a low gas superficial velocity and no big bubbles appear. The stability of oil in water-type slug flow results from the quasi-periodic movements between gas slug and liquid slug. The bubble-slug transitional flow occurs between the other two flow patterns and some big bubbles or big slugs stochastically appear in this flow pattern, leading to the large differences in conductance fluctuating signals among different data sets, correspondingly, the standard deviations of $S[-]$ of the transitional flow are relatively large.

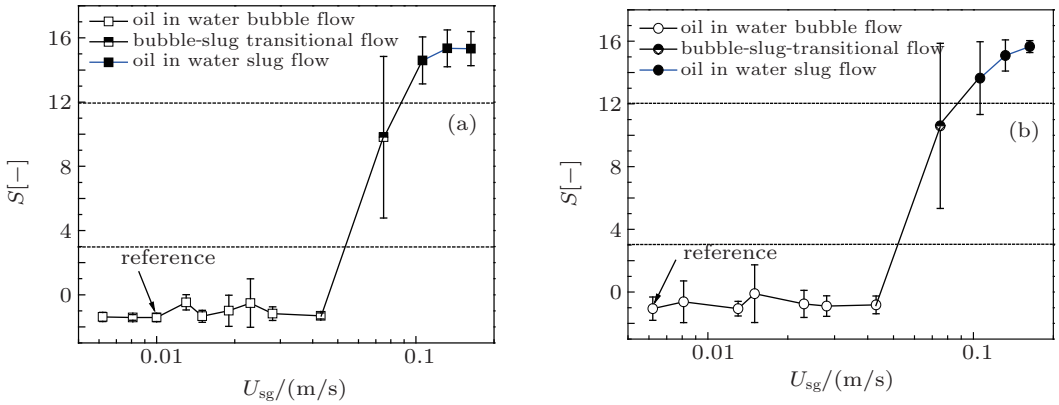


Fig. 7. Distributions of $S[-]$ with respect to gas superficial velocity in the cases of $Q_{mix} = 20$ m^3 per day and (a) $f_o = 10\%$ and (b) $f_o = 20\%$.

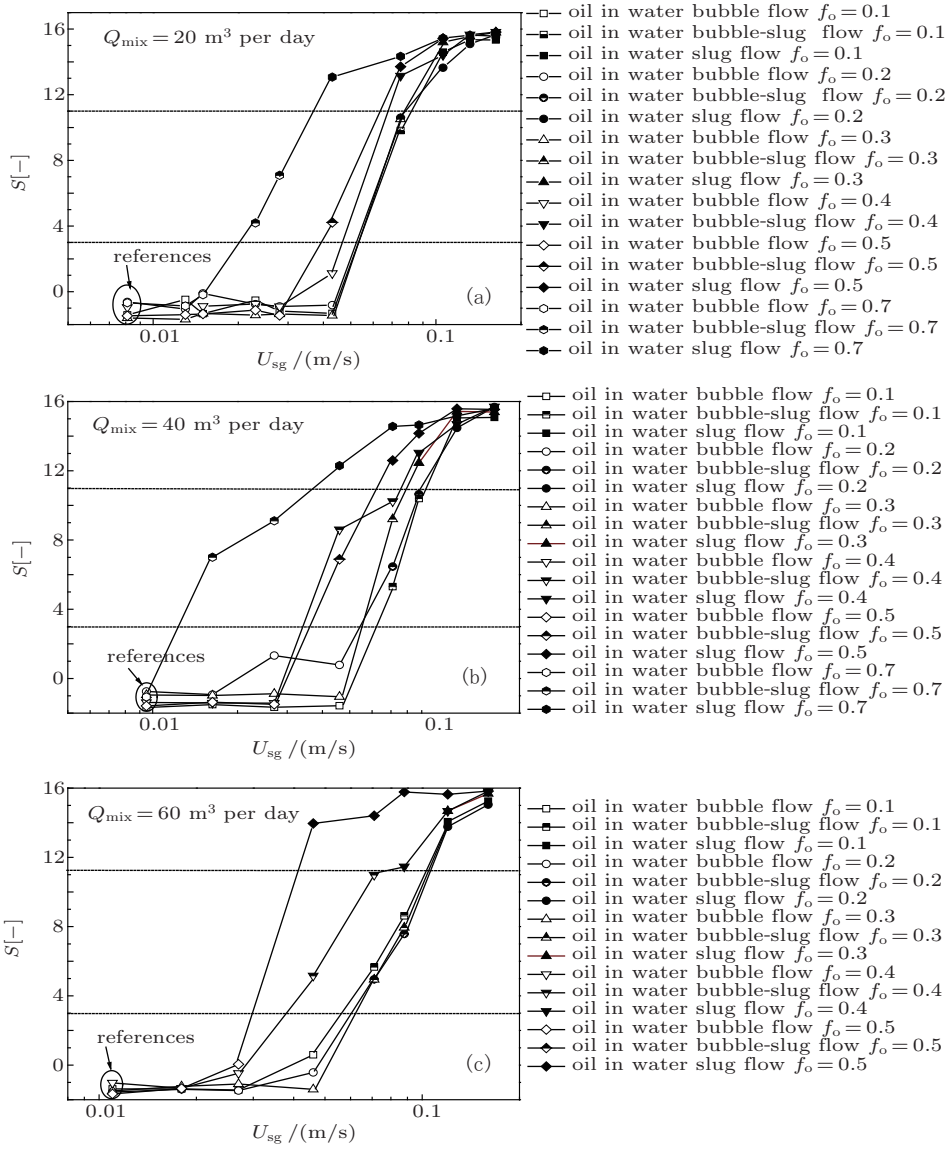


Fig. 8. (color online) Distributions of $S[-]$ with respect to gas superficial velocity with (a) $Q_{mix} = 20$ m^3 per day; (b) $Q_{mix} = 40$ m^3 per day; (c) $Q_{mix} = 60$ m^3 per day.

In Fig. 8, the flow conditions with the same mixture liquid flow rate ($Q_{\rm mix}$) and oil volume fraction ($f_{\rm o}$) are classified into a group. For each group, we choose the oil in water type bubble flow with the lowest gas superficial velocity as the reference flow condition, and then calculate the $S[-]$ values of each group. As shown in Fig. 8, for each group of flow conditions, the values of $S[-]$ for the oil in water-type bubble flows are all less than 3, and the $S[-]$ values for transitional flows are distributed in a range from 3 to 11, while the values of $S[-]$ for the slug flows are located in the area $S[-] > 11$.

The distributions of the statistic $S[-]$ in Fig. 8 further confirm that the flow conditions belonging to the same flow pattern possess a similar fluid mechanism, and a difference between two flow conditions will lead to a large $S[-]$, demonstrating the sensitiveness and effectiveness of the attractor comparison method.

4.2.2. Distributions of $S[-]$ with respect to oil volume fraction

Figure 9 shows the distributions of $S[-]$ with respect to oil volume fraction ($f_{\rm o}$) for a fixed mixture liquid flow rate and superficial gas velocity. We choose the flow conditions with the lowest oil volume fraction ($f_{\rm o}$) serving as the reference.

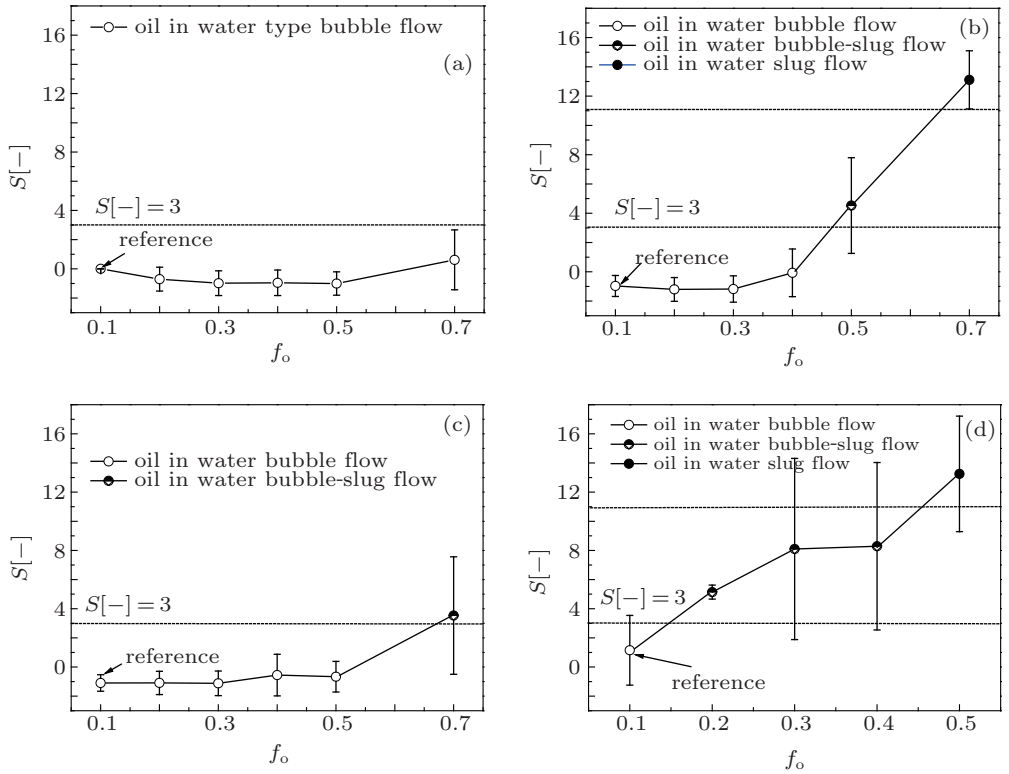


Fig. 9. Distributions of $S[-]$ with respect to oil volume fraction ($f_{\rm o}$), with (a) $Q_{\rm mix} = 20$ m^3 per day, $U_{\rm sg} = 0.0081$ m/s; (b) $Q_{\rm mix} = 20$ m^3 per day, $U_{\rm sg} = 0.043$m/s; (c) $Q_{\rm mix} = 40$ m^3 per day, $U_{\rm sg} = 0.0163$ m/s; (d) $Q_{\rm mix} = 60$ m^3 per day, $U_{\rm sg} = 0.071$ m/s.

We can see that with the increase of oil volume fraction ($f_{\rm o}$), the flow pattern evolves from oil in water-type bubble flow into a transitional flow and then finally into a slug flow. The $S[-]$ values of oil in water-type bubble flow are less than 3 and their standard deviations are relatively small, indicating the stability of this flow pattern. When the flow changes into a transitional flow pattern, the values of $S[-]$ are distributed in a range (3, 11), indicating the significant change of fluid mechanism, and the relatively large standard deviation of $S[-]$ suggests that there exist large differences between different data sets of the transitional flow. The values of $S[-]$ become even larger as the flow evolves into an oil in water-type slug flow, indicating the far greater difference compared with those of the other two flow patterns, and the relatively small standard deviations of $S[-]$ indicating the stability of slug flow pattern.

5. Conclusions

We investigate the dynamic characteristics of oil–gas–water three-phase flow by using the attractor comparison method. We first demonstrate how to properly determine calculation parameters, then we calculate the values of $S[-]$ for different flow conditions with the changes of gas superficial velocity and oil volume fraction ($f_{\rm o}$). The results suggest that the statistic $S[-]$ can effectively characterize the dynamical differences among oil in water-type bubble flow, transitional flow, and oil in water-type slug flow induced by the changes of the flow parameters.

Compared with the traditional nonlinear analysis method,

the statistic $S[-]$ considers complete probability distributions of the reconstructed attractor, and reserves the phase information of the attractor as much as possible, therefore it can effectively reflect the differences between dynamical attractors. In this regard, the attractor comparison method provides an effective analytical method of studying the dynamical mechanism of three-phase flow.

References

[1] Thorn R, Johansen G A and Hammer E A 1997 *Meas. Sci. Technol.* **8** 691

[2] Cazarez O, Montoya D, Vital A G and Bannwart A C 2010 *Int. J. Multiphase Flow* **36** 439

[3] Pao W K S and Lewis R W 2002 *Comput. Methods Appl. Mech. Engrg.* **191** 2631

[4] Padiala N T, VanderHeydena W B, Rauenzahna R M and Yarbrob S L 2000 *Chem. Eng. Sci.* **55** 3261

[5] Jones J O C and Zuber N 1975 *Int. J. Multiphase Flow* **2** 273

[6] Song C H, No H C and Chung M K 1995 *Int. J. Multiphase Flow* **21** 381

[7] Sun B, Wang E P and Zheng Y J 2011 *Acta Phys. Sin.* **60** 014701 (in Chinese)

[8] Du M, Jin N D, Gao Z K, Wang Z Y and Zhai L S 2012 *Int. J. Multiphase Flow* **41** 91

[9] Mi Y, Ishii M and Tsoukalas L H 2001 *Nucl. Eng. Des.* **204** 87

[10] Bai B F, Guo L J and Chen X J 2000 *Chin. J. Chem. Eng.* **51** 848

[11] Daw C S, Finney C E A, Vasudevan M, van Goor N A, Nguyen K, Bruns D D, Kostelich E J, Grebogi C, Ott E and Yorke J A 1995 *Phys. Rev. Lett.* **75** 2308

[12] Fan L T, Neogi D, Yashima M and Nassar R 1990 *AIChE J.* **36** 1529

[13] Gandhi A B, Joshi J B, Kulkarni A A and Jayaraman V K 2008 *Int. J. Multiphase Flow* **34** 1099

[14] Sæther G, Bendiksen K, Müller J and Frøland E 1990 *Int. J. Multiphase Flow* **16** 1117

[15] Hay J M, Nelson B H, Briens C L and Bergougnou M A 1995 *Chem. Eng. Sci.* **50** 373

[16] Wang Z Y, Jin N D, Gao Z K, Zong Y B and Wang T 2010 *Chem. Eng. Sci.* **65** 5226

[17] Llauró F X and Llop M F 2006 *Int. J. Multiphase Flow* **32** 1397

[18] Xiao N and Jin N D 2007 *Acta Phys. Sin.* **56** 5149 (in Chinese)

[19] Llop M F, Jand N, Gallucci K and Llauró F X 2012 *Chem. Eng. Sci.* **71** 252

[20] Diks C, van Zwet W R, Takens F and DeGoede J 1996 *Phys. Rev. E* **53** 2169

[21] van Ommen J R, Coppens M O, van den Bleek C M and Schouten J C 2000 *AIChE J.* **46** 2183

[22] Nijenhuis J, Korbee R, Lensselink J, Kiel J H A and van Ommen J R 2007 *Chem. Eng. Sci.* **62** 644

[23] Bartels M, Nijenhuis J, Lensselink J, Siedlecki M, de Jong W, Kapteijin F and van Ommen J R 2009 *Energy & Fuels* **23** 157

[24] Cao Y, Wang J, He Y, Liu W and Yang Y 2009 *AIChE J.* **55** 3099

[25] Villa J, van Ommen J R and van den Bleek C M 2003 *AIChE J.* **49** 2442

[26] Pukkelsheim F 1994 *Am. Stat.* **48** 88

[27] Jin N D, Zhao X, Wang J, Wang Z Y, Jia X H and Chen W P 2008 *Meas. Sci. Technol.* **19** 045403

[28] Takens F 1981 *Dynamical Systems and Turbulence* (Berlin: Springer Verlag) p. 366